Combustion and Flame 271 (2025) 113803

Contents lists available at ScienceDirect

Combustion and Flame

journal homepage: www.sciencedirect.com/journal/combustion-and-flame

Laser-induced plasma analysis of ammonia-oxygen and ammonia-oxygen-enriched-air flames at elevated pressures

Bilge Kaan Gokcecik, Nagaraju Guthikonda, Aleksander Clark, Peng Zhao, Zhili Zhang *

Department of Mechanical, Aerospace, and Biomedical Engineering, University of Tennessee, Knoxville, TN 37996, USA

ARTICLE INFO

Keywords:
Ammonia
Turbulent flame
Fuel-air ratio
Nanosecond
Laser-induced breakdown spectroscopy
High pressure

ABSTRACT

This study employed Laser-induced breakdown spectroscopy (LIBS) to measure the fuel-oxidizer ratio (FOR) of ammonia combustion with oxygen-enriched air and pure oxygen flames at elevated pressures (100 - 300 kPa). The correlations between the spectral line intensity ratios of nitrogen (N), hydrogen (H), oxygen (O), and equivalence ratio were used to quantify the FOR of flames at various pressures. The effect of pressure on the stability and precision of the calibration profiles for the elemental intensity ratios in flames was investigated. It was observed that the H/O correlation decreases with pressure increase for both ammonia flames. N/O correlations decrease with elevated pressure for the ammonia-oxygen flame. Furthermore, the nitrogen (N_{II}) spectral emission lines at 568 nm and 595 nm were used to estimate the plasma temperature, while the hydrogen (H_α) line at 656 nm was used for electron number density measurements.

1. Introduction

Ammonia has garnered substantial interest as a promising hydrogen-carrier alternative fuel due to several advantages. Its carbon-free structure is a primary advantage, making it a potential fuel for mitigating climate change. Furthermore, it can be produced with renewable energy sources (green ammonia production), resulting in no carbon-based greenhouse gas emissions during production as well [1]. Its low-pressure requirements at room temperature for transportation and storage make it manageable, safe, and economical. Moreover, its relatively low-cost production compared to other fuels enhances its appeal.

Despite these advantages, ammonia presents specific challenges and limitations [2]. It has a lower heating value than conventional fuels like gasoline and diesel [3], and it features high ignition temperature, narrow flammability range, low flame speed, and high heat of vaporization. However, several strategies can be developed to overcome ammonia's limited combustion aspects, including blending additional fuels, such as methane [4], dimethyl ether (DME) [5], and hydrogen [6,7], to help improve ammonia's combustion performance. Additionally, oxygen enrichment in the air enables the use of ammonia in broader equivalence ratios and higher pressures by enhancing the stability of the ammonia flame [8–10]. To address these challenges, further analysis of the combustion behavior of ammonia is still needed to develop efficient and clean combustion systems.

Several studies explored combustion properties of ammonia, such as mole fractions, laminar burning velocities, NO_x production concentrations, and ignition delay times [11,12]. Additionally, recent studies investigated diatomic emissions of ammonia flames such as NO, OH, and NH using chemiluminescence spectra [13,14]. Despite significant research on ammonia combustion flame parameters, a critical knowledge gap remains regarding its potential for elemental intensity and plasma analysis. Only a few studies on ammonia combustion dynamics use Laser-induced breakdown spectroscopy (LIBS). Zhang et al. investigated an ammonia-air flame with chemiluminescence and femtosecond-LIBS methods to measure unburned ammonia with NH/N_2 ratios [15]. Yang et al. [16] researched the vibrational excitation of ammonia plasma spectroscopy by using a CO_2 laser. They measured plasma temperature and electron density of plasma in different conditions with continuous CO_2 laser on and off mode and various delay times. Chen et al. [17] focused on determining the ammonia-oxygen mixture's probability density function at various laser energy and flame speeds.

This work employed LIBS to focus on ammonia flames for FOR measurements, elemental intensity ratios, and plasma properties to contribute literature. LIBS is a direct and versatile analytical technique used to determine the elemental composition of solids, liquids, and gases. Its user-friendly features, including straightforward setups, minimal data processing requirements, and elimination of sample

* Corresponding author.
E-mail address: zzhang24@utk.edu (Z. Zhang).

https://doi.org/10.1016/j.combustflame.2024.113803
Received 2 June 2024; Received in revised form 13 October 2024; Accepted 13 October 2024
Available online 17 October 2024

preparation steps, along with its ability to provide high spatial resolutions and rapid measurements, have led to widespread adoption across diverse scientific disciplines such as medicine, archaeology, aerospace, and agriculture. Its resilience in harsh, toxic, and challenging environments makes it particularly suitable for analyzing ammonia combustion processes as well.

LIBS provides a wealth of quantitative information on elemental composition, temperature, flame density, species concentration, and FOR measurements [18–28]. Due to high-intensity light scattering from the laser-induced plasma, LIBS offers superior elemental detection efficiency, multispecies concentration measurement, and a high signal-to-noise ratio. This makes it advantageous compared to other laser techniques like Raman scattering and fluorescence spectroscopy [29]. Especially for FOR measurement under elevated pressures and temperatures for ammonia flame, LIBS yields enhanced sensitivity, enabling the detection of a broader range of elements at lower concentrations.

This study investigated the application of nanosecond-LIBS (ns-LIBS) to ammonia flames due to the well-known advantages of the LIBS technique in this context. The paper is organized as follows: Section 3 explores the optimal combustion conditions, including oxygen ratio in air, maximum pressure, and delay time, for achieving stable and accurate LIBS measurements of the ammonia flame. Section 4 analyzes the elemental intensities and their ratios as a function of equivalence ratios. Section 5 presents measurements of plasma properties, including electron number density and plasma temperature. Section 6 concludes the paper, summarizing the findings of ns-LIBS for ammonia flame analysis.

2. Experimental Setup

The ns-LIBS experiments detailed in this study were conducted within a stainless-steel high-pressure combustion chamber, as illustrated in Fig. 1. The chamber has a 5.85-inch inner diameter, 25-inch height, and three 2-inch diameter glass windows for optical diagnostics. The chamber also has two inlet passages positioned near the base, facilitating the supply of fuel and oxidizer to a 1-inch diameter Hencken burner contained in the chamber. The exhaust valve at the top of the chamber expels the flame byproducts. All the ports were approximately 30 cm above the chamber's base and strategically aligned with the Henken burner flame. Two of the three fused silica window ports were used for laser beam focusing and collection of the LIBS spectra, and an inlet flow opening was dedicated to continuously purging the internal glass windows and the chamber with air. Air purging is necessary to prevent water condensation on glass windows that might obstruct the laser beam propagation and maintain the overall chamber pressure. A corrosion-resistant flow meter (ALICAT-Ms-5SLPM) and a stainless-steel sensitive needle are employed to withstand the corrosive nature of ammonia. Two digital mass flow controllers adjust air and oxygen flow rates.

A Nd: YAG laser (Powerlite DLS, Continuum Inc.) beam at 1064 nm wavelength, 200 mJ/pulse energy, 8 ns pulse duration with 10 Hz repetition rate was used to generate LIBS plasma inside the ammonia flame. A spherical convex lens of focal length of 100 mm inside a chamber port with a glass window focuses the laser beam 2 cm above the Hencken burner surface. It creates ellipsoidal-shaped plasma with hundreds of micrometers in width and a few millimeters in length. The emissions from the plasma were collected by a combination of achromatic lenses with $f = 150$ mm focal length (one inside the chamber port and the other outside the chamber) and focused onto the 500 μm entrance slit of the spectrometer (SpectraPro HRS-300, Princeton Instruments). The spectrometer was equipped with a 150-groove/mm grating blazed at 500 nm and mounted to an electron-multiplying charge-coupled device (EMCCD) camera (ProEM HS:1024BX3, Princeton Instruments) of 1024 × 512 pixels array. The spectrometer was centered at 680 nm wavelength, covering a wavelength region of 530 – 830 nm. The laser system and EMCCD camera were externally triggered by a digital delay generator (Stanford Research Systems, DG645) to control the time between the laser pulse and signal collection (i.e., the gate delay). The EMCCD was operated at T_{delay}= 40 ns gate delay, 20 ns exposure time, 30 MHz electron multiplied mode, and the analog gain was configured at a low mode with 16-bit depth to record 500 images of the LIBS spectrum. The short camera exposure and gate delay time were chosen to suppress/attenuate the flame chemiluminescence and increase the signal-to-noise ratio by avoiding strong Rayleigh scattering and stray light scattering.

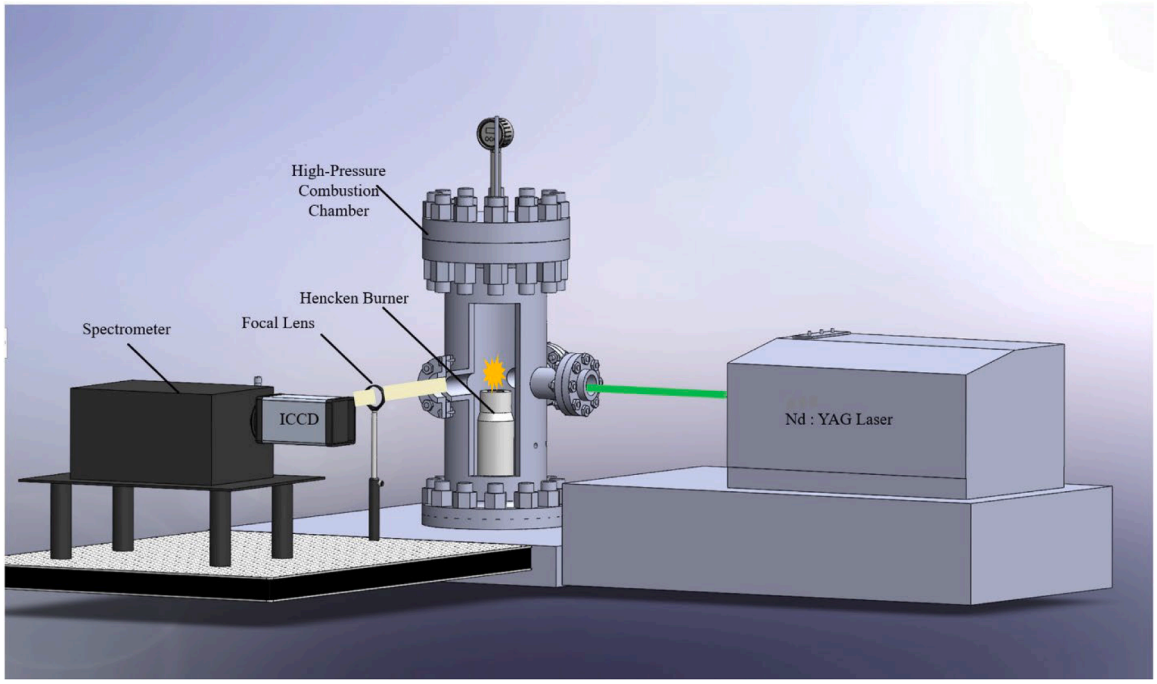

Fig. 1. Experimental setup for ns-LIBS from ammonia flames.

3. Fine-tuning combustion parameters for stable ammonia flame

Achieving consistent combustion of ammonia fuel in the Hencken burner at atmospheric and room temperature proves challenging due to ammonia's lower heating value (18.8 MJ/kg), high autoignition temperature (651°C), and lower flame speed. Even if the flame can achieve stability under atmospheric pressure and stoichiometric conditions, it tends to blow out as pressure increases and the equivalence ratio varies. In addressing this issue, previous studies have explored that secondary fuels like methane and hydrogen are often mixed with ammonia or utilized for thermal co-flow to enable sufficient heat for continuous ignition and faster flame speed to ensure a stable flame.

Another approach involves enhancing the stability of the ammonia flame by oxygen enrichment. Compared to secondary fuel addition, oxygen hinders the additional elemental analysis of spectra and the contribution of H and N elements from the secondary fuel in the spectra. For instance, analyzing the FOR for a flame of ammonia and methane through intensity ratios of elements becomes challenging. This is because H elements are derived from ammonia and methane, and N originates from air and ammonia. Considering all of these, oxygen enrichment is adopted in this study, making it feasible to conduct LIBS measurements of ammonia at elevated pressures.

The balanced chemical reaction in the theoretical complete combustion limit of ammonia-oxygen is:

$$4\ NH_3 + 3\ O_2 \rightarrow 6\ H_2O + 2\ N_2$$

This equation indicates that for every 4 moles of ammonia, 3 moles of oxygen are required. In this study, instead of using the required 3 moles of oxygen, 1.8 moles of O_2 and $1.2 \times 4.76 = 5.71$ moles of air were utilized. In the initial stages, the oxygen ratio in the air was systematically increased to achieve a stable flame in the burner. The elevated oxygen levels enabled fuel utilization at broad-range equivalence ratios. Forty percent oxygen concentration in the air was found effective in facilitating the combustion of ammonia in the Hencken burner, even under 6 bars. The oxygen ratio in this air is about 40 %, higher than the normal atmospheric condition (21 %).

Although the study initially aimed to conduct LIBS measurements at high pressures up to 6 bars, properties of ammonia restrain this intention. The low boiling temperature of gaseous ammonia poses a concern, causing it to transition into a liquid state under room temperature and high pressures. The inlet line requires pressurizing before introducing gaseous ammonia into the pressure chamber to ensure its smooth passage. The flow needle on the inlet line also acts as a throttle valve, requiring more pressure in the inlet to work properly. High pressures in the supply line and sudden pressure drops in the valve are responsible for causing liquid ammonia and leading to the liquid ammonia getting stuck in the flow meter, resulting in flow failure for equivalence measurement. Additionally, ammonia usage inside the pressure chamber generates significant water vapor, especially at elevated pressures. Due to the lower heating value of ammonia, the heat inside the chamber cannot vaporize the water sufficiently. The cold walls and cells of the chamber contribute to excessive water condensation, resulting in water droplets on the flame and burner. Moreover, the intense water production at elevated pressures disrupts the plasma emission spectrum and causes background interference with peaks. Due to these challenges and the need for precise data, this work was conducted at pressures up to 3 bars.

Furthermore, to establish the optimal delay time for FOR measurements employing a 200 mJ/pulse laser, we experimented with different delay times using a methane-air flame, building upon previous research [23]. This experimentation determined that our work's most effective delay time is 40 ns. To streamline our study, we focused on LIBS-based measurements of ammonia-oxygen and ammonia-oxygen-enriched-air flames within the 1 – 3 bars pressure range, employing a gate delay of T_{delay}= 40 ns.

4. Results and discussion

4.1. Analysis of LIBS spectrum

The study of plasma emission using the Hencken burner reveals elemental analysis of ammonia combustions. Fig. 2 displays averaged plasma spectrum at various equivalence ratios for different pressures (100 – 300 kPa). The combustion LIBS spectra consist of Nitrogen ionic lines (N_{II}) at 568 nm and 595 nm, a Nitrogen atomic line (N_I) at 746 nm, a dominant Hydrogen (H_α) line at 656 nm, and an Oxygen line (O_I) at 777 nm in the observed wavelength region. All the spectral emission lines in the spectrum were identified with the help of the NIST atomic database [30]. All LIBS emission spectrum line intensities were prone to fluctuations due to the probabilistic behavior of the laser-induced gas breakdown process, fluctuations in the laser energy and light transmission through the optical elements, etc. To optimize transmission of all optical elements, the spectrometer was calibrated using Princeton Instruments' standard calibration lamp (IntelliCal, Hg and Ne/Ar dual switchable USB light source) in the 530 nm - 830 nm wavelength range with an RMS error = 0.04 nm, which greatly improves the spectral collection efficiency. The calibration LIBS spectrum was not corrected for flame emissions to represent the effect of chemiluminescence and flame byproducts effect on the spectrum baseline as shown in Fig. 2. To maintain the better signal-to-noise ratio (SNR), the experiment was repeated 500 times at the same experimental conditions, i.e., laser energy, equivalence ratio, gate delay, and gate width. To evaluate the experimental uncertainties in the plasma properties, the baseline corrected 500 spectra were divided into 5 average spectra (each spectrum was an average of 100 spectra) at an equivalence ratio for a pressure condition.

Fig. 2 (a-c) and 2 (d-f) depict the plasma spectra (without flame emissions correction), observed from the ammonia-oxygen-enriched-air and ammonia-oxygen flames, respectively. The baseline corrected spectra used for the analysis was shown in supplementary information (Fig. S1) for both the flames. As the fuel-to-oxidizer ratio (equivalence ratio, Φ) transitions from lean to rich flows, the average spectral emissions of the plasma decrease at atmospheric pressure but increase at elevated pressures for both flames. Notably, the H_α peak emerges prominently, exhibiting slight broadening at elevated pressures for both flames. Additionally, the atomic spectrum of N_I at 746 nm experiences augmentation with increasing pressures, particularly pronounced in the ammonia-oxygen-enriched-air flames due to the contribution of N molecules from air compared to the ammonia-oxygen flame. The variation of N, O and H elements intensity with the equivalence ratio at different pressure was shown in supplementary information (Fig. S2) for both the flames. At elevated pressures, the baseline of the ammonia-oxygen-enriched-air flame decreases at higher wavelengths due to the continuum spectral bands of NO_2 and NH_2 α-bands contribution between 550 - 650 nm [11,15]. Ammonia-oxygen combustion offers the flexibility of expanding the fuel equivalence ratio limits from 0.6 to 1.4 compared to the ammonia-oxygen-enriched-air flame, which has limits of 0.7 – 1.3.

4.2. Fuel oxidizer ratio measurements from ns-LIBS spectrum

The analysis of FOR in ammonia-oxygen-enriched-air and ammonia-oxygen combustions relies on specific elemental peaks: N_{II} (568 nm), O_I (777 nm), and H_α (656 nm). Fig. 3 (a-i) illustrates calibration curves for the N_{II}/O_I, H_α/O_I and N_{II}/H_α ratio ratios used to FOR measurements at different pressures for the ammonia-oxygen-enriched-air combustion.

For the ammonia-oxygen-enriched air flames, the measurements of N_{II}/H_α ratio decrease with the equivalence ratio at 100 kPa and varies non-monotonously at higher pressure (200 – 300 kPa). The decreasing trend of the N_{II}/H_α ratio at 100 kPa may be attributed to the flame quenching due to higher laminar burning velocity of ammonia at increased fuel ratio (Φ) [31] and the non-monotonous behavior at

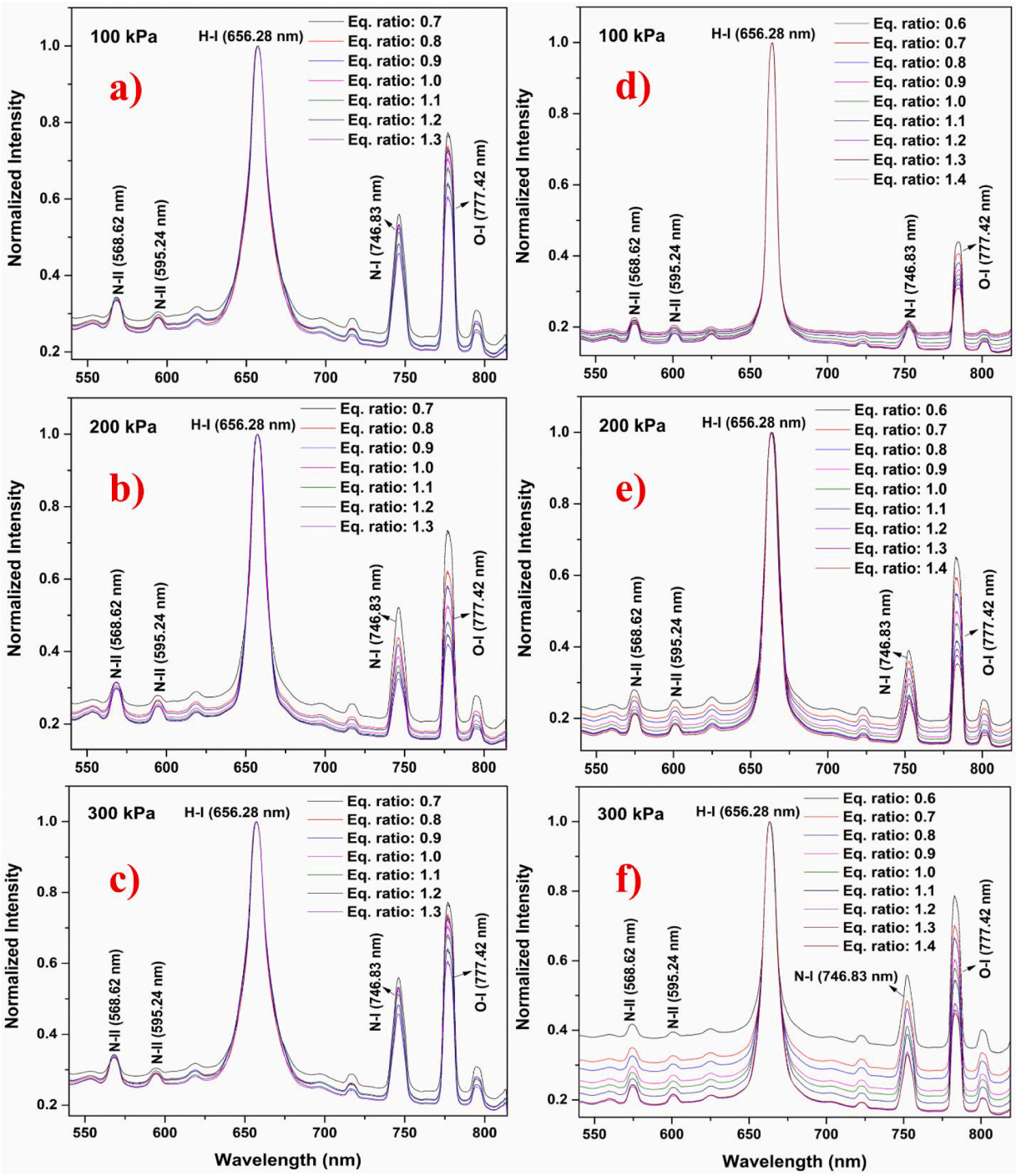

Fig. 2. The LIBS spectrum (without flame emissions/baseline correction) from ammonia flames with (a-c) oxygen-enriched-air and (d-f) oxygen with different equivalence ratios (Φ) at 100 – 300 kPa.

higher pressure (200 – 300 kPa) may arise from the nonlinear increase of the emission line intensity due to the collisional broadening at higher pressures [32] and overlapping contribution of N from NH_3 and air. However, the N_{II}/O_I ratio calibration curves were linear due to the oxygen enrichment of the ammonia-air fuel. The N_{II}/O_I ratio as a function of the equivalence ratio does not distinguish between individual nitrogen sources, only providing the total content and the collisional broadening of emission elements at higher pressure ($\geq$ 200 kPa) [32], which reduced the coefficient of determination (R^2) value for the linear fit of calibration curves. So, both the N_{II}/H_α and N_{II}/O_I ratios were impractical for FOR measurements due to the overlapping nitrogen contribution from both NH_3 and air. Conversely, the H_α/O_I ratios were meaningful with higher R^2 (> 99 mJ) value, because the air contains neglectable hydrogen inside it (0.000055 mJ) [33]. So, the H_α only contributed from Ammonia, O_I from both the air and added oxygen. Therefore, the H_α/O_I ratio was the only reliable indicator for ammonia-oxygen-enriched-air analysis.

Fig. 4 (a-i) illustrates calibration curves for the N_{II}/O_I, H_α/O_I and N_{II}/H_α ratios used to FOR measurements at different pressures for the ammonia-oxygen combustion. The presence of both N_{II} (568 nm) and H_α (656 nm) exclusively from ammonia enhances the accuracy of FOR assessments of both N/O and H/O intensity ratios as a function of

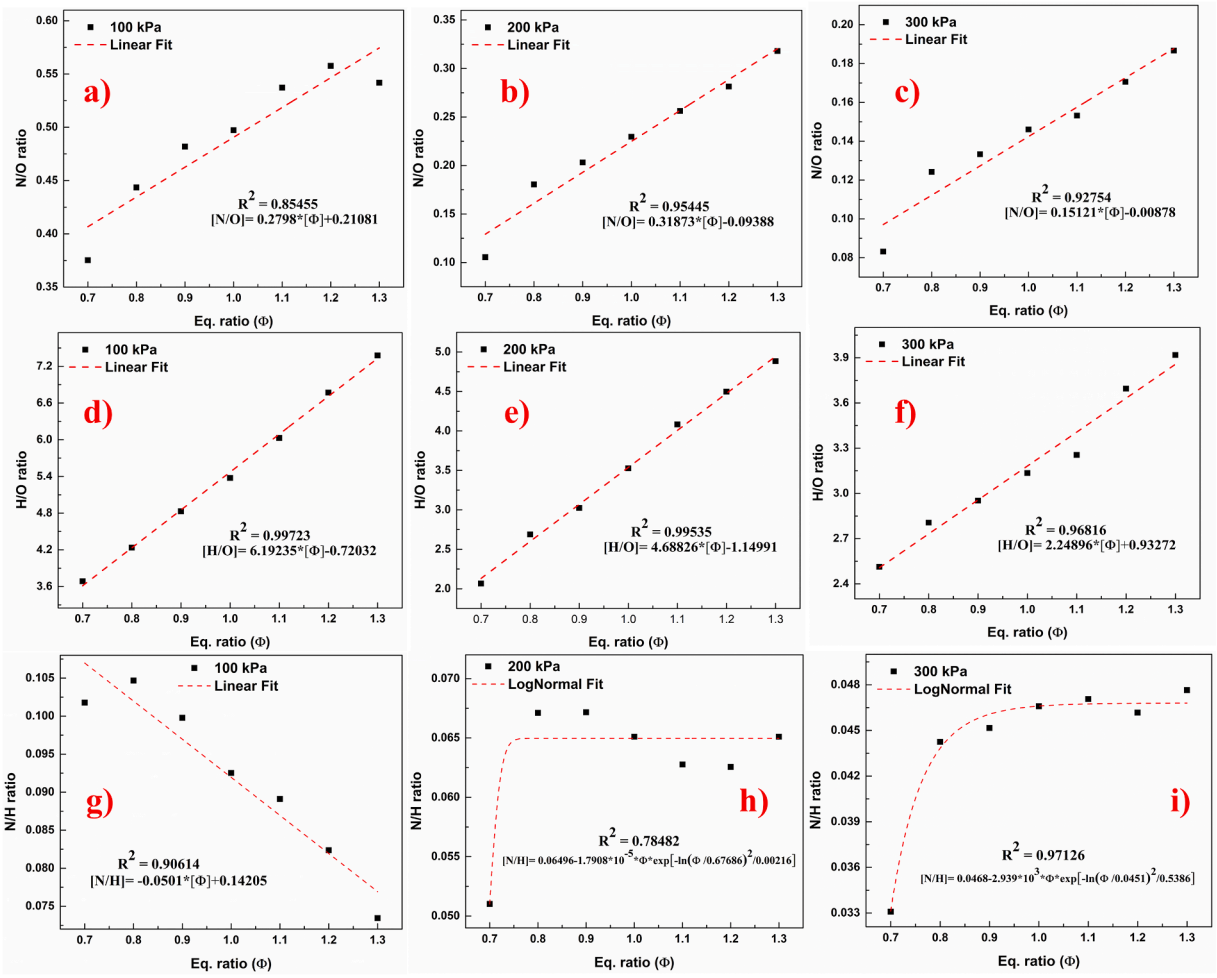

Fig. 3. Calibration curves of FOR measurements for ammonia-oxygen-enriched-air flames.

equivalence ratio at various pressures. In contrast to the ammonia-oxygen-enriched-air flame, the N_{II} and H_α exclusively originate from NH_3 and O_I (777 nm) is solely derived from oxygen, making both the N_{II}/O_I and H_α/O_I ratios reliable indicators for the ammonia-oxygen analysis at different pressures. Notably, The R^2 value for both N_{II}/O_I and H_α/O_I ratio was decreased at higher pressure due to the collisional broadening of emission elements at higher pressure ($\geq$ 200 kPa) [32] similar to the ammonia-oxygen-enriched-air flames. Although N_{II} and H_α emissions were exclusively from ammonia, the N_{II}/ H_α ratio was decreased at 100 kPa due to flame quenching caused by the higher laminar burning velocity of the ammonia fuel [31]. At high pressures the N_{II}/ H_α ratio was decreased until $\Phi = 1.1$ and later, it was increased more linearly. This may be due to the laminar burning velocity for ammonia, which increases with equivalence ratio and attains maximum at $\Phi = 1.1$, and later decreases [31], So the N_{II}/ H_α ratio was attained linearity after $\Phi = 1.1$. Therefore, the N_{II}/O_I and H_α/O_I ratios were more reliable indicators for the ammonia-oxygen flames at different pressures.

5. Plasma temperature (T_e) and electron number density (n_e) measurements for plasma properties

Plasma temperature is a critical thermodynamic property that governs various plasma characteristics, including the molecular distribution across energy levels, the relative abundance of different ionization states, optical thinness, electron number density, and the overall behavior of the plasma. Two primary methods are prevalent in measuring plasma temperature: line intensity ratio and the Boltzmann plot method. With its exceptional precision and extensive use in the LIBS community, the Boltzmann plot method stands out as the preferred approach here. This method leverages the analysis of multiple spectral lines emitted by the same element in the same ionization state. By considering the known transition probabilities, degeneracies, and upper energy levels of these lines, the Boltzmann plot technique enables us to determine the plasma temperature graphically.

Under Local Thermal Equilibrium (LTE), the intensity of a spectral line is directly related to the population of the corresponding energy level, as described by the following equation:

$$I = \frac{hcN_0}{4\pi\lambda}(g_k A_{ki})\left(\frac{e^{\frac{-E_k}{k_B T_e}}}{U(T_e)}\right) \quad (1)$$

Applying log normal to the above equation (1)

$$ln\left(\frac{I\lambda}{g_k A_{ki}}\right) = \frac{-E_k}{k_B T_e} + ln\left(\frac{hcN_0}{4\pi U(T_e)}\right) \quad (2)$$

The plot of $ln\left(\frac{I\lambda}{g_k A_{ki}}\right)$ against E_k yields a slope of $\frac{-1}{k_B T}$, providing the plasma temperature (T_e). where I represents the emission line intensity, λ - wavelength, g_k - degeneracy in excited transition level, A_{ki} - spontaneous Einstein emission coefficient, E_k - energy of the excited state, k_B - Boltzmann constant, $U(T_e)$ - partition function, h - Planck's constant, and c - the speed of light in vacuum.

Accurate determination of plasma temperature using the Boltzmann plot method relies on careful selection of emission lines. Choosing distinct lines well-separated from neighboring lines minimizes overlapping spectral features and ensures reliable intensity measurements.

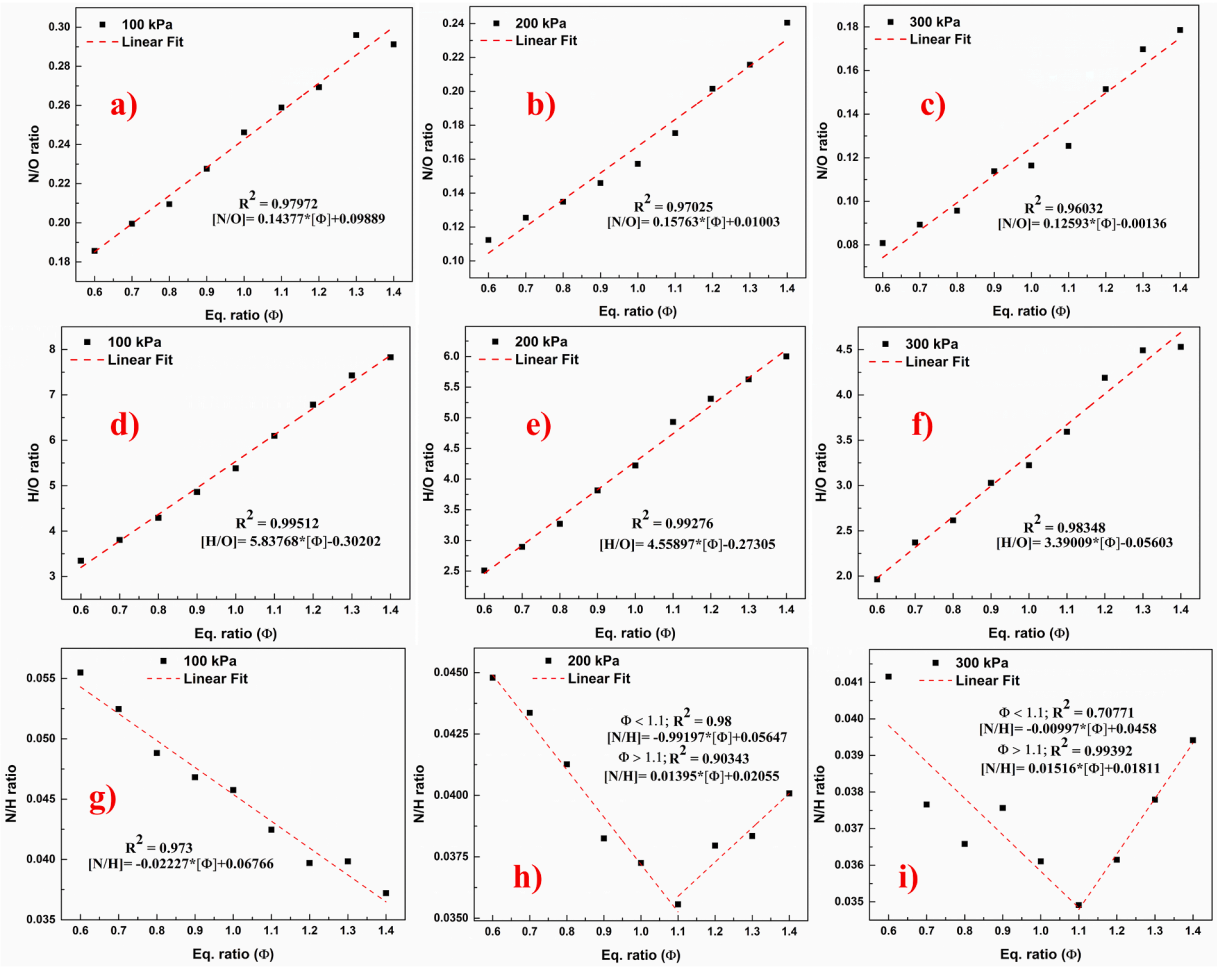

Fig. 4. Calibration curves of FOR measurements for ammonia-oxygen flames.

Furthermore, integrating the area under the spectral envelope provides a more accurate representation of the total emission intensity than solely relying on peak height measurements, which can be susceptible to noise or baseline fluctuations. Therefore, in this study, baseline-corrected emission lines of nitrogen and N_{II} at 568 nm and 595 nm, along with their corresponding spectroscopic parameters from Table 1, were substituted into Equation (2) to obtain Boltzmann plots for calculating the plasma temperature.

The Electron number densities were determined by fitting the Lorentzian profile to the Stark broadening profile (width) of the H_α line (656 nm) and substituting it in the Griem expression [34];

$$n_e = \left(\frac{\Delta\lambda_{1/2}}{2w}\right) \times 10^{16} \quad (in\ cm^{-1})$$

Where $\Delta\lambda_{1/2}$ represents full width at half maximum (FWHM), and w is the electron impact width parameter.

The variation of T_e with equivalence ratio (Φ) at various pressures is depicted in Fig. 5(a) and Fig. 5(c) for ammonia-oxygen-enriched-air and ammonia-oxygen flames, respectively. The maximum T_e of approximately 2.27 ± 0.023 eV was observed for the ammonia-oxygen-enriched-air flame at Φ = 0.7 and 100 kPa pressure, while for the ammonia-oxygen flame, the maximum T_e of roughly 2.20 ± 0.014 eV at Φ = 0.6 and 100 kPa. At 100 kPa pressure, as the equivalence ratio (Φ) increased, the T_e decreased with a slope of approximately 0.14 eV and 0.16 eV for ammonia-oxygen-enriched-air and ammonia-oxygen flames, respectively. At 200 kPa pressures, the T_e increased with a slope of 0.79 eV and 0.35 eV, while at 300 kPa pressure, it increased with a slope of 0.39 eV and 0.57 eV, respectively. Although T_e increased with equivalence ratio (Φ) at higher pressures, it remained lower than the T_e observed at 100 kPa for both flames except for the ammonia-oxygen flame, where the maximum T_e was observed for Φ > 1.1 at 200 kPa.

Fig. 5 (b & d) illustrates the variation of electron number densities of ammonia-oxygen-enriched-air and ammonia-oxygen flames with equivalence ratio (Φ) at various pressures. At atmospheric pressure, the electron number density (n_e) decreased with an increasing fuel ratio, exhibiting linear slopes of 3.09×10^{-17} cm^{-3} and 9.9×10^{-16} cm^{-3} for both flames. As pressure increases, the Doppler broadening of the hydrogen spectrum enhances electron number density. At elevated pressures, higher fuel ratios result in increased concentrations of target species near the focal region, leading to a greater interaction cross-section of the laser beam and, consequently, higher electron number densities. The trend in electron number density mirrors that of plasma temperature. However, for the ammonia-oxygen flame at elevated pressures, electron number density experiences a slight decrease after Φ > 1.1. The maximum n_e of approximately 3.65×10^{18} cm^{-3} is observed for the ammonia-oxygen-enriched-air flame at Φ = 1.2 under atmospheric pressure. Conversely, the maximum n_e of approximately 2.21 ×

Table 1
The spectroscopic parameters of the NH_3 combustion spectrum.

Species	NIST λ (nm)	E_k (eV)	E_i(eV)	A (s^{-1})	g_k	g_i
N-II	568.621	20.646058	18.466228	1.78E07	3	3
	595.239	23.242271	21.159916	1.24E07	5	5
N-I	746.831	11.9955753	10.3358956	1.96E07	4	6
H-I	656.279	12.0875052	10.1988358	4.4101E07	18	8
O-I	777.417	10.7402250	9.1460911	3.69E07	5	5

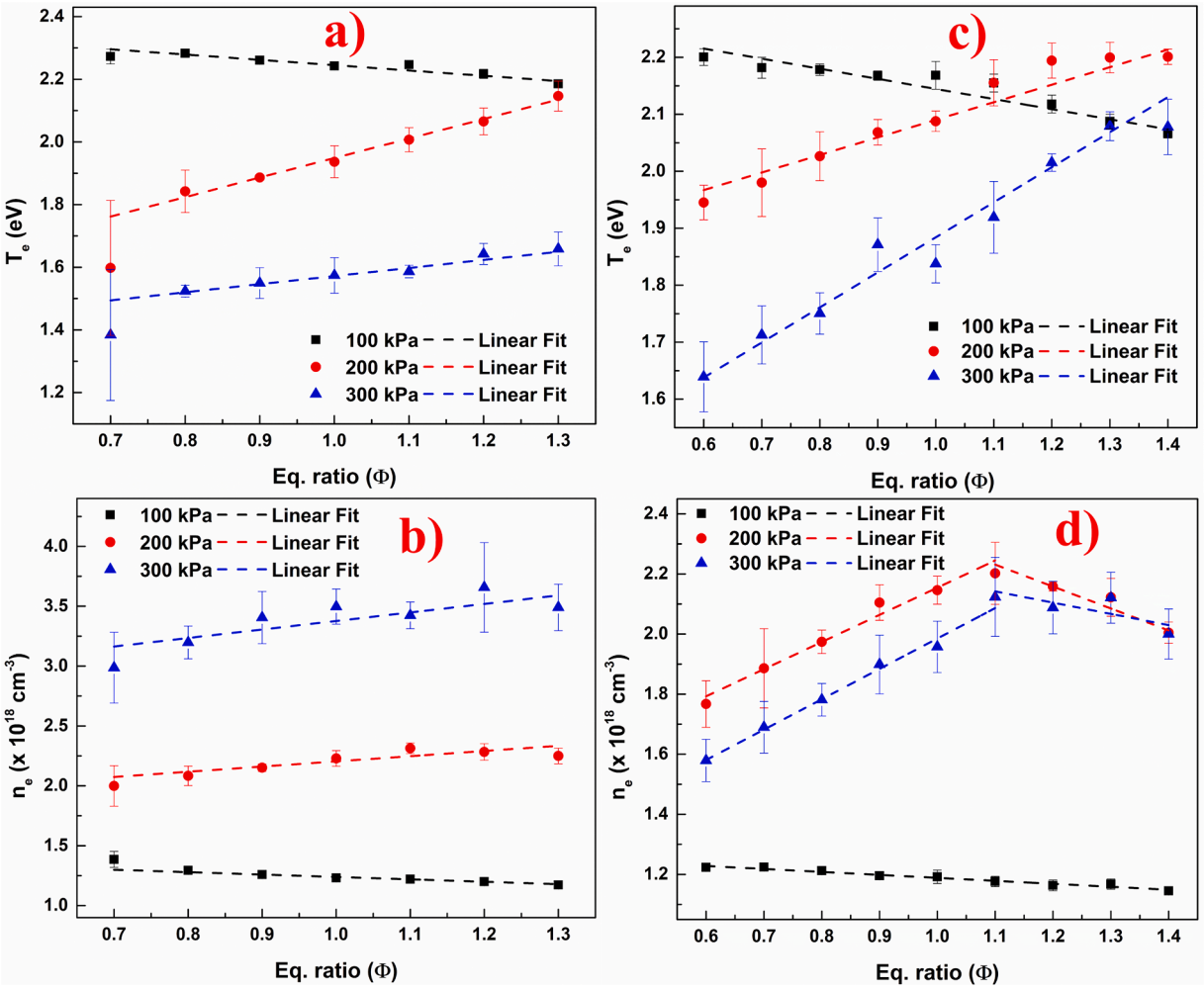

Fig. 5. Variation of Plasma Temperature (T_e) and Electron number densities (n_e) as functions of Equivalence ratio (Φ) at different pressures for (a-b) ammonia-oxygen-enriched-air and (c-d) ammonia-oxygen flames.

10^{18} cm^{-3} was observed at Φ = 1.1 under 200 kPa pressure for the ammonia-oxygen flame.

6. Summary and conclusions

The ns-Laser-induced plasma spectrums of ammonia flames were analyzed, resulting in very accurate fuel-air ratio measurements using the elemental intensity ratio of the LIBS for ammonia-oxygen-enriched-air and ammonia-oxygen flames. The spectral emissions of nitrogen and hydrogen were utilized to calculate the plasma temperature and electron number density. The following conclusions can be drawn from the results presented here:

(1) The emission spectra of the ammonia-oxygen-enriched-air flame were elevated over the range of 550 – 650 nm due to continuous spectra of NO_2 and NH_2 α-bands. In contrast, ammonia-oxygen flames lack this elevation, indicating that oxygen usage as an oxidizer result in fewer chemiluminescence signals and/or byproducts.
(2) The H/O intensity ratio is more efficient than the N/O ratio for measuring FOR in an ammonia-oxygen-enriched-air flames due to overlapping N contribution from both NH_3 and air. However, the H/O and N/O ratio remains valid for the ammonia-oxygen flames as the ammonia was the only source contributed to H and N.
(3) The N/H ratio was not at all useful for both the flames as the ammonia laminar burning velocity plays a crucial role in the complete dissociation of the NH_3 fuel.
(4) The calibration curves R^2 value was decreased at high pressure (200 – 300 kPa) due to the collisional broadening of atoms independent of the pressure at high pressure (≥ 200 kPa).
(5) In the ammonia-oxygen flames, the N/H ratio was linear after Φ > 1.1 at higher pressures due to the low ammonia laminar burning velocity.
(6) Plasma temperature and electron number density exhibit similar linear trends under all pressure conditions, except for the electron number density of an ammonia-oxygen flame, which shows a decreasing trend after the point at the equivalence ratio 1.1 at elevated pressures.

Novelty and significance

Accurate quantification of the fuel-oxidizer Ratio (FOR) of Ammonia is essential for optimizing combustion efficiency, reducing pollutant emissions, and improving safety and reliability. LIBS is a valuable technique for FOR measurement due to its ability to perform nonintrusive, local point measurements with high temporal and spatial resolutions, enabling rapid and real-time analysis. This study addresses three key investigations: firstly, it pioneers using LIBS to measure FOR in ammonia flames at various pressures. Secondly, it deviates from conventional approaches by using pure oxygen instead of secondary fuels to

enhance ammonia's chemical reactivity. Finally, it provides valuable reference points for future research by measuring plasma number density and electron temperature for different equivalence ratios at varying pressures. In conclusion, this study demonstrates a novel application of LIBS for ammonia flames with oxygen-enriched air and pure oxygen, bridging a critical gap in existing knowledge and offering valuable insights into ammonia combustion dynamics.

CRediT authorship contribution statement

Bilge Kaan Gokcecik: Writing – review & editing, Writing – original draft, Investigation, Formal analysis. **Nagaraju Guthikonda:** Writing – review & editing, Data curation. **Aleksander Clark:** Writing – review & editing. **Peng Zhao:** Writing – review & editing. **Zhili Zhang:** Writing – review & editing, Supervision, Funding acquisition, Conceptualization.

Declaration of competing interest

The authors declare that they have no known competing financial interests or personal relationships that could have appeared to influence the work reported in this paper.

Acknowledgment

This research was supported by NSF and DOE.

Supplementary materials

Supplementary material associated with this article can be found, in the online version, at doi:10.1016/j.combustflame.2024.113803.

References

[1] G. Chehade, I. Dincer, Progress in green ammonia production as potential carbon-free fuel, Fuel 299 (2021) 120845.
[2] D. Erdemir, I. Dincer, A perspective on the use of ammonia as a clean fuel: challenges and solutions, Int. J. Energ. Res. 45 (2021) 4827–4834.
[3] K. Ryu, G.E. Zacharakis-Jutz, S.C. Kong, Effects of gaseous ammonia direct injection on performance characteristics of a spark-ignition engine, Appl. Energ. 116 (2014) 206–215.
[4] J. Wang, X.Z. Jiang, K.H. Luo, Exploring reaction mechanism for ammonia/methane combustion via reactive molecular dynamics simulations, Fuel 331 (2023) 125806.
[5] T. Cai, D. Zhao, Enhancing and assessing ammonia-air combustion performance by blending with dimethyl ether, Renew. Sust. Energ. Rev. 156 (2022) 112003.
[6] W. Liang, C.K. Law, Enhancing ammonia combustion using reactivity stratification with hydrogen addition, P. Combust. Inst. 39 (2023) 4419–4426.
[7] A.H. Bakir, H. Ge, Z. Zhang, P. Zhao, Autoignition enhancement of ammonia spray under engine-relevant conditions via hydrogen addition: thermal, chemical, and charge cooling effects, Int. J. Engine Res. 24 (2023) 3970–3984.
[8] M. Ilbas, O. Kekul, A. Bektas, S. Karyeyen, Oxidizer effects on ammonia combustion using a generated non-premixed burner, Int. J. Hydrogen Energ. 47 (2022) 12317–12337.
[9] Y. Zhu, H.J. Curran, S. Girhe, Y. Murakami, H. Pitsch, K. Senecal, L. Yang, C. W. Zhou, The combustion chemistry of ammonia and ammonia/hydrogen mixtures: a comprehensive chemical kinetic modeling study, Combust. Flame 260 (2024) 113239.
[10] S. Wang, A.M. Elbaz, Z. Wang, W.L. Roberts, The effect of oxygen content on the turbulent flame speed of ammonia/oxygen/nitrogen expanding flames under elevated pressures, Combust. Flame 232 (2021) 111521.
[11] A. Hayakawa, Y. Hirano, E.C. Okafor, H. Yamashita, T. Kudo, H. Kobayashi, Experimental and numerical study of product gas characteristics of ammonia/air premixed laminar flames stabilized in a stagnation flow, P. Combust. Inst. 38 (2021) 2409–2417.
[12] H. Kobayashi, A. Hayakawa, K.D.K.A. Somarathne, E.C. Okafor, Science and technology of ammonia combustion, P. Combust. Inst. 37 (2019) 109–133.
[13] X. Zhu, W.L. Roberts, T.F. Guiberti, UV-visible chemiluminescence signature of laminar ammonia-hydrogen-air flames, P. Combust. Inst. (2022). S1540748922000517.
[14] W. Weng, M. Aldén, Z. Li, Visible chemiluminescence of ammonia premixed flames and its application for flame diagnostics, P. Combust. Inst. (2022). S1540748922002814.
[15] D. Zhang, Q. Gao, B. Li, J. Liu, Y. Tian, Z. Li, Femtosecond laser-induced plasma spectroscopy for combustion diagnostics in premixed ammonia/air flames, Appl. Optics 58 (2019) 7810.
[16] G. Yang, L. Liu, T. Wang, L. Fan, X. Huang, D. Tian, L. Jiang, J.F. Silvain, Y. Lu, Laser-induced breakdown spectroscopy of ammonia gas with resonant vibrational excitation, Opt. Express 28 (2020) 1197.
[17] Y.L. Chen, J.W.L. Lewis, C. Parigger, Probability distribution of laser-induced breakdown and ignition of ammonia, J. Quant. Spectrosc. Ra. 66 (2000) 41–53.
[18] T.X. Phuoc, F.P. White, Laser-induced spark for measurements of the fuel-to-air ratio of a combustible mixture, Fuel 81 (2002) 1761–1765.
[19] J. Kiefer, B. Zhou, Z. Li, M. Aldén, Impact of plasma dynamics on equivalence ratio measurements by laser-induced breakdown spectroscopy, Appl. Optics 54 (2015) 4221.
[20] Y. Ren, A. Kreischer, F. Cameron, H. Pitsch, Quantitative measurement of mixture fraction in counterflow diffusion flames by laser-induced breakdown spectroscopy, Combust. Flame 241 (2022) 112130.
[21] Y. Wu, M. Gragston, Z. Zhang, P.S. Hsu, N. Jiang, A.K. Patnaik, S. Roy, J.R. Gord, High-pressure 1D fuel/air-ratio measurements with LIBS, Combust. Flame 198 (2018) 120–129.
[22] M. Gragston, P. Hsu, N. Jiang, S. Roy, Z. Zhang, Emissions in short-gated ns/ps/fs-LIBS for fuel-to-air ratio measurements in methane-air flames, Appl. Optics 60 (2021) C114.
[23] P.S. Hsu, M. Gragston, Y. Wu, Z. Zhang, A.K. Patnaik, J. Kiefer, S. Roy, J.R. Gord, Sensitivity, stability, and precision of quantitative Ns-LIBS-based fuel-air-ratio measurements for methane-air flames at 1–11 bar, Appl. Optics 55 (2016) 8042.
[24] M. Gragston, P. Hsu, A. Patnaik, Z. Zhang, S. Roy, Time-Gated Single-Shot Picosecond Laser-Induced Breakdown Spectroscopy (ps-LIBS) for Equivalence-Ratio Measurements, Appl. Spectrosc. 74 (2020) 340–346.
[25] M.B. Shattan, M. Gragston, Z. Zhang, J.D. Auxier, K.G. McIntosh, C.G. Parigger, Mapping of Uranium in Surrogate Nuclear Debris Using Laser-Induced Breakdown Spectroscopy (LIBS), Appl. Spectrosc. 73 (2019) 591–600.
[26] Y. Wu, M. Gragston, Z. Zhang, C.D. Smith, P.S. Hsu, N. Jiang, S. Roy, J.R. Gord, Time-gated Line-LIBS for fuel/air ratio measurements at elevated pressures, in: 2018 AIAA Aerospace sciences meeting, American Institute of Aeronautics and Astronautics, Kissimmee, Florida, 2018.
[27] A.K. Patnaik, P.S. Hsu, Y. Wu, M. Gragston, Z. Zhang, J.R. Gord, S. Roy, Ultrafast laser-induced-breakdown spectroscopy (LIBS) for F/A-Ratio measurement of hydrocarbon flames, in: 2018 AIAA Aerospace sciences meeting, American Institute of Aeronautics and Astronautics, Kissimmee, Florida, 2018.
[28] A.K. Patnaik, Y. Wu, P.S. Hsu, M. Gragston, Z. Zhang, J.R. Gord, S. Roy, Simultaneous LIBS signal and plasma density measurement for quantitative insight into signal instability at elevated pressure, Opt. Express 26 (2018) 25750.
[29] M.M. Tripathi, K.K. Srinivasan, S.R. Krishnan, F.Y. Yueh, J.P. Singh, A comparison of multivariate LIBS and chemiluminescence-based local equivalence ratio measurements in premixed atmospheric methane–air flames, Fuel 106 (2013) 318–326.
[30] Atomic spectra database, NIST, 2009. https://www.nist.gov/pml/atomic-spectra-database.
[31] J. Li, S. Lai, D. Chen, R. Wu, N. Kobayashi, L. Deng, H. Huang, A review on combustion characteristics of ammonia as a carbon-free Fuel, Front. Energy Res. 9 (2021) 760356.
[32] T.X. Phuoc, Optics and Lasers in Engineering 44 (2006) 520–534.
[33] Earth Fact Sheet, (n.d.). https://nssdc.gsfc.nasa.gov/planetary/factsheet/earthfact.html.
[34] H.R. Griem, Plasma Spectroscopy, McGraw-Hill, 1964.